



ELSEVIER

Tectonophysics 323 (2000) 131–148

TECTONOPHYSICS

www.elsevier.com/locate/tecto

Shear zones in the Proterozoic lithosphere of the Arabian Shield and the nature of the Hales discontinuity

Vadim Levin *, Jeffrey Park

Department of Geology and Geophysics, Yale University, New Haven, CT 06520, USA

Received 3 December 1999; accepted for publication 4 April 2000

Abstract

Seismic velocity discontinuities are commonly found within the upper 100 km of the mantle lithosphere, with great variability in their depth, lateral extent, and the polarity of velocity jump. Among the more commonly observed is the ‘80 km’ or Hales discontinuity, identified in a variety of tectonic environments, and sometimes associated with seismic anisotropy. Teleseismic receiver functions for Global Seismographic Network station RAYN on the eastern edge of the Arabian Shield contain a strong converted-phase P_{HS} that we believe arises from the Hales discontinuity at the depth of 70 km. On the basis of the polarization, azimuthal behavior and frequency dependence of P_{HS} , we characterize the Hales discontinuity as marking an upper boundary of a zone of depth-dependent anisotropy within the upper mantle. The RAYN receiver functions indicate a similar zone at the crust-mantle transition at 40 km. Forward modeling in simple one-dimensional anisotropic models indicates that the receiver functions require, assuming hexagonal anisotropy, an inclined symmetry-axis with N–S strike. In our preferred model there are two anisotropic zones bounded, respectively, by the sharp Moho and the Hales discontinuities on the top. Smooth gradients of anisotropic properties extend beneath the discontinuities. Within both zones the anisotropic symmetry axes, indicative of systematic fabric in the olivine-dominated upper mantle material, are oriented along the N–S direction ($\pm 10^\circ$), and are tilted from the vertical 50° toward the south. We propose that these regions of coherent fabric within the upper mantle represent shear zones developed during late Proterozoic continent–continent collision, when the Ar-Rayn tectonic block underwent northward ‘escape’ along the northern flank of the Najd fault system. © 2000 Elsevier Science B.V. All rights reserved.

Keywords: Arabian Shield; Hales discontinuity; orogeny; receiver functions; seismic anisotropy; terrane accretion

1. Introduction

The Hales discontinuity, one of several weak interfaces in the upper mantle, is observed intermittently at depths between 60 and 100 km, and has uncertain origin. First noted in active-source

refraction seismic profiles as an inflection of the P and S traveltime curves at 500–800 km offset (Hales, 1969; Hales et al., 1975; Fuchs and Vinnik, 1982; Pavlenkova, 1996), it also can appear as a reflector beneath the Moho in continental regions (Benz and McCarthy, 1994; Bellefleur et al., 1997). ScS reverberations (Revenaugh and Jordan, 1991), S-to-P conversions that precede various teleseismic S phases (Zhang and Lay, 1993; Earle et al., 1994), shear-coupled P waves (Zandt and Randall, 1985), and P-to-S conversions in teleseismic receiver func-

* Corresponding author. Tel.: +1-203-432-3279;
fax: +1-203-432-3134.

E-mail addresses: vadim@geology.yale.edu (V. Levin),
park@geology.yale.edu (J. Park)

tions (RF) (Bostock, 1997, 1998; Sandvol et al., 1998) indicate that the Hales, or '80 km,' discontinuity is widespread globally, in both continental and oceanic regions.

Mantle discontinuities in the 50–100 km depth range have been variously attributed to the petrologic transition from spinel peridotite to garnet peridotite (Hales, 1969), anisotropy from localized shear zones (Fuchs, 1983) and shallow low velocity zones (Benz and McCarthy, 1994) speculatively caused by pervasive partial melt (Thybo and Perchuc, 1997). Noting that the Hales discontinuity beneath the Canadian Slave province appears as a sharply bounded layer of width 10 km, Bostock (1998) proposes a hybrid model of localized shear developed within Archean oceanic crust as it undergoes the gabbro-to-eclogite phase transition during shallow subduction. Bostock's model for the Hales, if applicable generally in continental regions, would validate the slab-accretion model for the formation of continental lithosphere (e.g. Abbott, 1992), as it would imply that buoyant trapping of shallow-subducting slabs by the retardation of the gabbro-to-eclogite phase transition (Sacks, 1983) is pervasive in the Earth's tectonic history.

To determine whether the Hales has one primary cause in continental regions, or develops via a number of mechanisms, the discontinuity must be imaged in a variety of geotectonic settings. In this paper we study its behavior beneath the Arabian Shield, using seismic records from 85 events recorded at station RAYN (Ar Rayn, Saudi Arabia) of the Global Seismographic Network (GSN). Teleseismic RFs (Langston, 1981; Kosarev et al., 1984; Ammon, 1991; Gurrola et al., 1995) offer a good tool for investigation, as the amplitude variation of P-to-S converted waves with back azimuth, particularly on the transverse-horizontal component, is a clear diagnostic of anisotropy at a buried interface (Levin and Park, 1997b, 1998; Bostock, 1997, 1998; Savage, 1998).

In the next section, we outline tectonic controversies concerning the Arabian Shield, as currently understood. In Section 3 we present RFs for station RAYN and test models for the Moho and Hales discontinuities, consistent with the existence of localized shear zones dating from the late

Paleozoic. Section 4 discusses possible geotectonic models for this behavior. Section 5 summarizes our conclusions.

2. Geotectonic setting: central Arabia

The Arabian–Nubian shield (ANS) was assembled in the late Proterozoic (900–600 Ma) at the climax of the Pan-African orogeny (Stoeser and Camp, 1985; Abdelsalam and Stern, 1996; Berhe, 1997), a clear example of the 'plate tectonic' style of continental accretion (Stern, 1994). The ANS consists primarily of several distinct 'juvenile' crustal terranes from the late Proterozoic, identified as either oceanic plateaus or island arcs (Ibrahim and McCourt, 1995; Abdel-Rahman, 1995; Stein and Goldstein, 1996), often bordered by ophiolites. Evidence of some Archean crust has been found on the southern edge of the Arabian peninsula (Windley et al., 1996; Whitehouse et al., 1998), suggesting continuity with the Mozambique belt to the south. Bentor (1985) identifies four stages of volcanism preserved in the shield that can be related to a Wilson orogenic cycle: emplacement of mafic rocks associated with a growing ocean basin (starting at 900 Ma), the formation of andesitic island arcs (up to 640 Ma), felsic batholith formation upon continental collision (640–600 Ma), and post-orogenic alkaline volcanism (600–540 Ma). The patchwork of Proterozoic terranes was overprinted with a N–S trend of volcanism in its western half during the late Cenozoic (Camp and Roobol, 1992). During the Proterozoic postorogenic stage, the convergence of a continental fragment from the east led the crust of central Arabia to develop the Najd fault system of NW-trending strike-slip faults to accommodate E–W compression, while allowing N–S extension in the form of an escaping block (Stern, 1994). Several of the terranes that comprise modern Arabia are exposed in the western peninsula, eastern Egypt and northeastern Sudan, but the outlines of buried terranes can be discerned beneath the Phanerozoic sediments of the Arabian Platform by their geomagnetic signature (Johnson and Stewart, 1995). Station RAYN (Ar-Rayn, Saudi Arabia) of the global seismic network is sited on

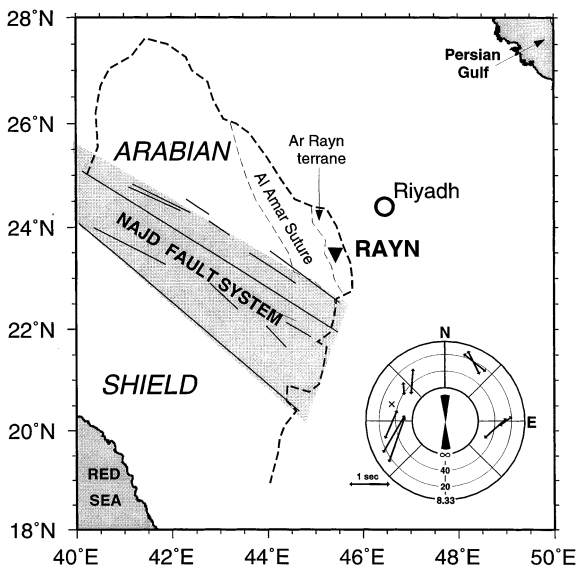


Fig. 1. Location of the Global Seismic Network station RAYN (▼) with respect to the regional tectonic features of the Arabian Peninsula. The tectonic sketch is adapted from Stoesser and Camp (1985). The inset plots shear-wave splitting observations (see text and Table 2) on the polar diagram as a function of backazimuth and phase velocity. The arrows are aligned with the fast direction and scaled with the splitting delay. The center of the polar plot shows the range of possible orientations for anisotropic fast-axis strike within two upper-mantle zones identified through RF analysis.

an exposed corner of the Ar-Rayn terrane (Fig. 1) that is now largely covered by sediments.

From seismic refraction studies on the Shield in central and southwest Arabia (Mooney et al., 1985; Prodehl, 1985; Badri, 1991), the crust of the Ar-Rayn terrane is 40–45 km thick and has a strong uninterrupted Moho boundary. This crustal thickness is consistent with the receiver-function studies of Sandvol et al. (1998) and Al-Amri (1999). Rodgers et al. (1999) derived a 36 km crustal thickness for the shield from regional surface wave dispersion and waveform modeling. The surface-wave paths used by Rodgers et al. (1999) sample the Shield to the northwest of RAYN, while the refraction lines sample to the southwest, so this disagreement may be due to lateral variation.

Reflective/refractive boundaries in the uppermost mantle have been suggested by the refraction studies, but there is weak agreement among them.

Using stacked radial-component RFs for portable broadband stations in southwestern Arabia, Sandvol et al. (1998) found a Ps converted phase from a lithospheric interface below the Moho, whose depth and prominence vary greatly. Evidence for a Hales-like interface was not found, however, from data collected at the future site of RAYN.

The tectonic history of the Arabian–Nubian shield is complicated by conflicting evidence. Global surface wave tomography models consistently place a low-velocity anomaly under the Red Sea rift (e.g. Zhang and Tanimoto, 1993), suggesting that an upwelling plume currently erodes the Arabian lithosphere. This interpretation is consistent with uplift of the shield at ~14 Ma and with petrologic data from late Cenozoic volcanism (Camp and Roobol, 1992). Igneous rocks erupted in the ANS since the Precambrian, however, are consistently ‘enriched’ in geochemical tracers, suggesting no contribution from asthenospheric or late-stage plume melting (Stein and Goldstein, 1996). Moreover, geochemical models for trace-element transport in the neighborhood of a dehydrating slab suggest that large volumes of metasomatized lithosphere beneath Arabia have persisted unaltered since the assembly of the shield (Stein et al., 1997).

Upper mantle seismic anisotropy may reflect the fossil fabric of the lithosphere and offer clues to its tectonic history. Elastic anisotropy in deformed mantle peridotite can be caused by the lattice-preferred orientation (LPO) of olivine crystals (Zhang and Karato, 1995). Large shear-wave splitting (~1 s) from a temporary network of broadband seismometers in southwestern Arabia (Wolfe et al., 1999) suggests a uniform N–S fast axis of anisotropy across several crustal terranes. A similar uniformity of upper-mantle strain across distinct crustal terranes has been noted by Levin et al. (2000) for the northeastern United States. In Arabia the fast axis is parallel to the ancient orogen, in agreement with many orogens globally (Silver, 1996). If caused by olivine LPO, a uniform mantle fabric beneath the Arabian shield would likely have formed after its assembly, in a mantle tectonic event that preserved the heterogeneity of the surface geology. A broad mantle strain could

reflect the flow of asthenospheric material to replace the loss of a thickened mantle root during postorogenic tectonism (540–600 Ma), as proposed for Tibet (Molnar et al., 1993). Similar mantle strains could develop from slab rollback (Willett and Beaumont, 1994), also proposed for Tibet, or continental delamination, a mechanism proposed for the Basin-and-Range province of North America by Bird (1979). Strain associated with continental rifting is a less plausible cause, as the splitting fast axes of Wolfe et al. (1999) are neither parallel nor perpendicular to the Red Sea rift.

Because shear-wave splitting has minimal depth resolution, Wolfe et al. (1999) note that present-day drag at the base of shield would also fit their data. Progressive replacement of continental lithosphere by a southward-migrating plume since 14 Ma (e.g. Bonavia et al., 1995) might also produce the required mantle strain and anisotropy. Bonavia et al. (1995) argue that the late Cenozoic Red Sea plume may be responsible for mafic underplating of the ANS crust, which is evident in both the 1980s refraction surveys and in regional surface wave modeling (Rodgers et al., 1999). Another option is that mafic underplating occurred during postorogenic uplift as shield formation concluded, as a consequence of erosive uplift, delamination or loss of a thickened mantle root (Meissner and Mooney, 1998).

How can a study of the Hales discontinuity beneath a single broadband seismometer in central Arabia help resolve these issues of tectonic history? No definitive answer is likely, but different models lead to different predictions. At one extreme, if the Bostock (1998) Slave-province model for the Hales applies to Arabia and the lithosphere has truly remained undisturbed since terrane assembly, one might expect an anisotropic layer with an E–W fast axis to match the fossil E–W vergence of Proterozoic slabs. At another extreme, if anisotropic mantle fabric beneath the ANS is due entirely to recent plume activity, the Hales discontinuity may be absent altogether. Alternatively, it might mark the boundary of a region where anisotropic properties are at variance with the deeper mantle strain.

The inferences that we draw from RAYN RFs

do not follow either of these extremes, and lead us to an alternate scenario.

3. Impedance structure of the uppermost mantle

We use records of earthquakes at teleseismic distances observed at RAYN between January 1997 and July 1999 (Fig. 2). Broadband seismic data used in this study is collected with a Geotech KS-54000 borehole seismometer. Observational conditions at RAYN are exceptionally good, with very low ambient noise.

The simplest way to estimate a RF is by spectral division, a ratio of Fourier transforms for the different components: $H_R(f) = Y_R(f)/Y_Z(f)$ and $H_T(f) = Y_T(f)/Y_Z(f)$. Here $Y_Z(f)$, $Y_R(f)$ and $Y_T(f)$ are the Fourier spectra of the vertical, radial and transverse seismic components, respectively. An inverse Fourier transform converts spectral-domain RFs $H_R(f)$ and $H_T(f)$ into a prediction filter of Ps scattered waves. RFs are typically contaminated by the ‘scattered’ wave field, the portion of the P-wave coda that arises from

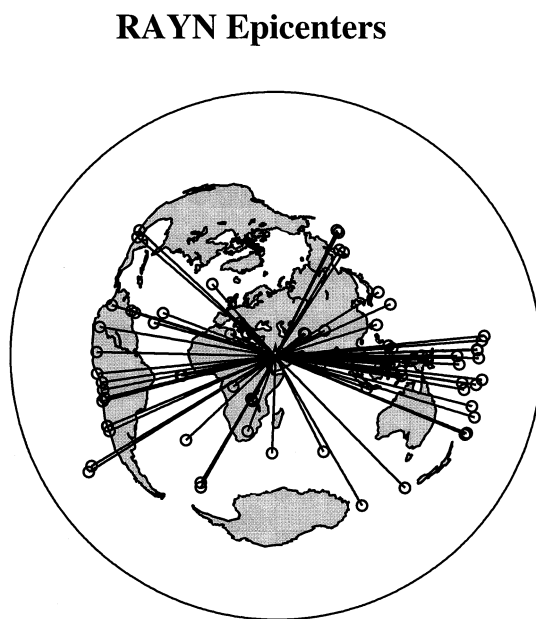


Fig. 2. Distribution of the 85 earthquakes (○) used in the RF analysis. The global polar projection is centered on station RAYN.

multiple scattering and conversion in a strongly heterogeneous crust (Abers, 1998). In this study we apply a new RF-estimation technique (Park and Levin, 2000) that uses multiple-taper spectral correlation estimates instead of spectral ratios. The multitaper algorithm has two distinct advantages. First, it estimates the RFs $H_R(f)$ and $H_T(f)$ only from the portion of the horizontal motion that is correlated (in a narrow frequency band) with the vertical motion. Second, the relative proportion of uncorrelated horizontal motion, as quantified by the spectral coherences $C_R(f)$ and $C_T(f)$, is used to estimate the uncertainty of $H_R(f)$ and $H_T(f)$. (High coherence implies low uncertainty.) These uncertainties can be used to weight RF-estimates from different earthquakes when estimating a composite, or ‘stacked’, RF in the frequency domain. There is no formal uncertainty estimate for the time-domain multitaper RF, but an informal assessment can be made from the acausal part of the RF, that is, the amplitude of $H_R(t)$, $H_T(t)$ for $t < 0$. In our experience with real data, the coherence between horizontal and vertical motion in a P coda is highly frequency dependent, and the pattern of frequency dependence can vary greatly from event to event. Therefore the use of uncertainty-based weights in multiple-record RF estimation is important.

In the frequency domain, RFs with associated uncertainty estimates can be developed usefully up to $f = 3\text{--}5$ Hz, even for teleseismic body waves whose frequency content is dominated by $f < 1$ Hz. If we assume a 0.125 s km^{-1} slowness difference between P and S waves and maximum resolution $f = 4$ Hz, one can hope for a 1 km half-wavelength resolution of interface width. Park and Levin (2000) show that Ps converted phases from the Moho beneath the GSN station ARU (Arti Settlement, Russia) approach this nominal resolution. We are able to extend the common practice of RF analysis, by employing teleseismic phases like PKP and P_{diff} in addition to direct P phases, to bolster the azimuthal coverage and to extend the range of phase velocities observed.

3.1. Observations

To create images in Fig. 3(A) we formed averages of frequency-domain RFs from earth-

quakes falling within backazimuthal bins 10° wide, with 50% overlap, so that each observed earthquake influences two adjacent bins. Contributions to the bin average from individual earthquakes are weighted by the inverse variances of RF estimates (Park and Levin, 2000). Similarly, Fig. 3(B) was created by averaging frequency-domain RFs from earthquakes in overlapping 10° epicentral distance bins, using earthquakes with backazimuths $45\text{--}115^\circ$. Fig. 3(B) shows that for a chosen range of directions the initial 10–12 s of the transmissivity response are consistent throughout the range of source-receiver distances.

Fig. 4 presents RF stacks computed in narrow backazimuth ranges for a variety of cutoff frequencies. To create a stack, frequency-domain RFs from a chosen backazimuthal range are bin-averaged with epicentral distance, and converted into the time domain. The composite time-domain RFs are stacked, resulting in a single time series. The eastern stack [Fig. 4(A)] is computed from data from backazimuths $75\text{--}105^\circ$, while the western stack is computed from data from backazimuths $255\text{--}285^\circ$. The time-trace RFs in Fig. 4 are used as data in forward modeling efforts discussed in the following section.

A strong phase, designated P_{MS} , is seen at 4.7 s on average. The phase is prominent in the high-frequency response, which suggests that it is associated with a first-order discontinuity in impedance structure. It arrives roughly at the same time from all backazimuths, and has no significant moveout with epicentral distance. This phase is explained well by a planar interface at depth. On the basis of timing we associate this phase with the crust–mantle interface.

The transverse component of P_{MS} is prominent between backazimuths 25° and 120° , and, with an opposite polarity, between backazimuths 220° and 290° . A two-lobed pattern like this in the absence of a prominent tilt on the interface indicates that seismic properties on at least one side of the interface are anisotropic (Levin and Park, 1998).

Another phase, designated P_{HS} , arrives between 6 and 8 s. The radial component of this phase is most prominent if the spectrum of the RF is limited at 1 Hz. The transverse component contains considerable energy at frequencies up to

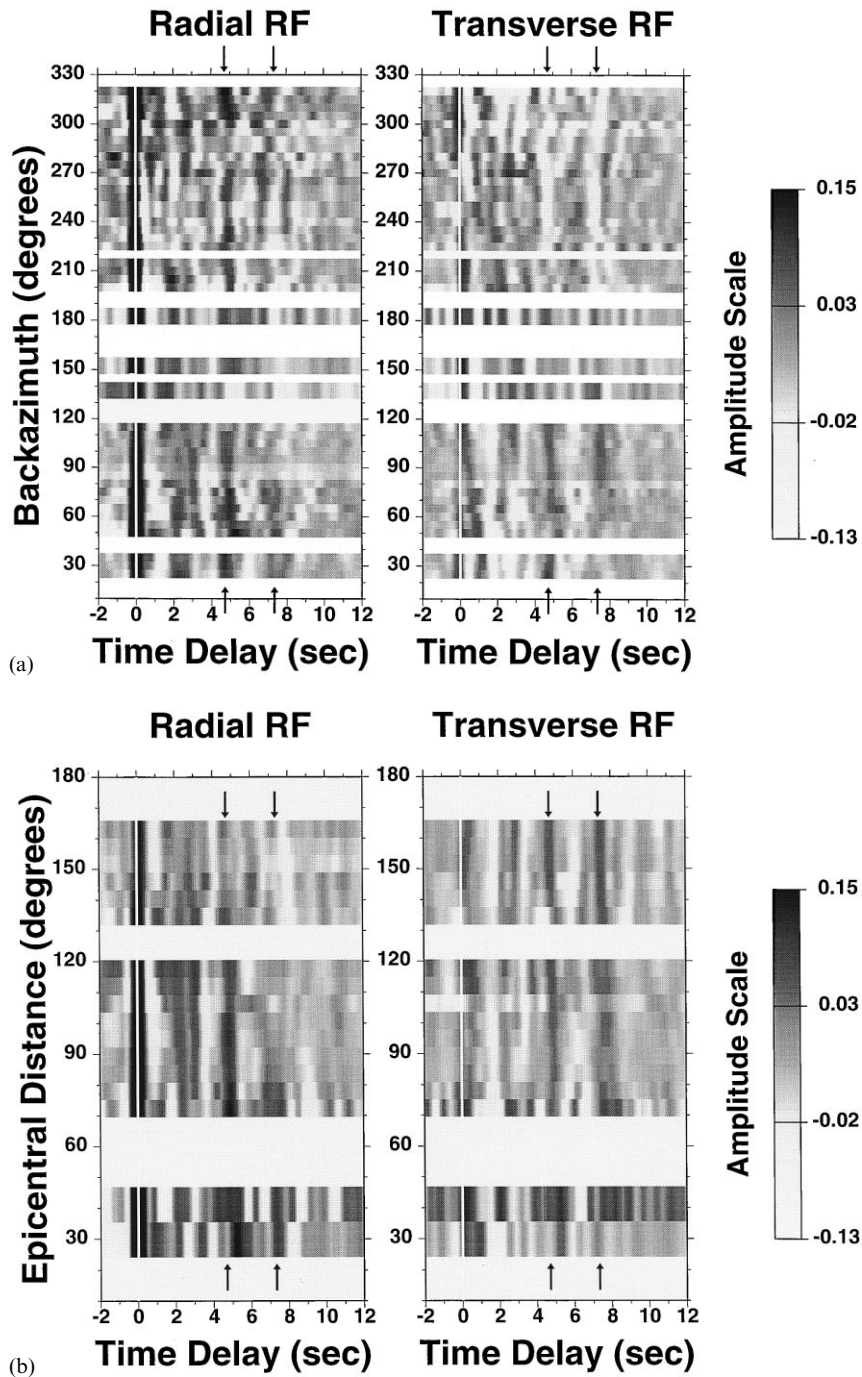


Fig. 3. Transmissivity response images (RFs) computed for RAYN (Ar-Rayn, Saudi Arabia) presented as a function of backazimuth (A) and as a function of epicentral distance (B). Data used include direct P, PKP and P_{diff} phases observed between spring of 1997 and summer of 1999. RF spectra are limited at 1 Hz. Epicentral-distance plot includes data from the backazimuthal range $45\text{--}115^\circ$. Phases P_{Ms} and P_{Hs} are identified by arrows. Note the polarity changes in the transverse RFs between eastern and western directions.

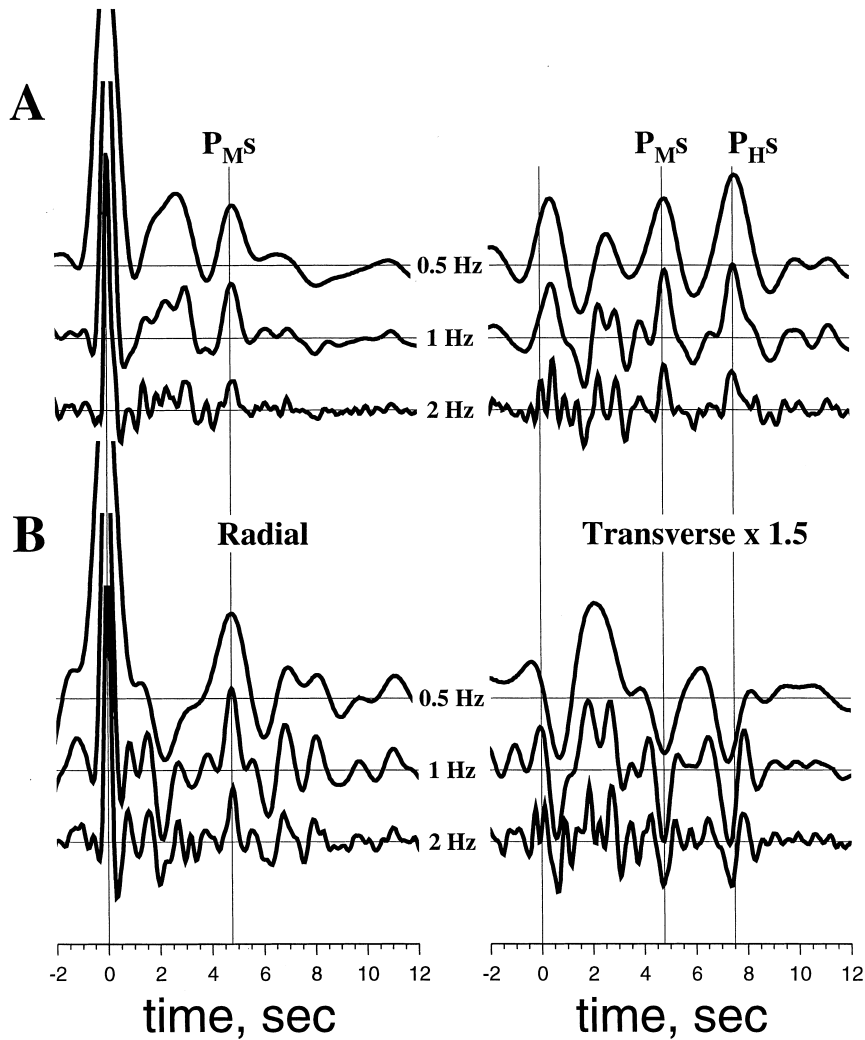


Fig. 4. Waveforms of composite RFs computed by stacking all RFs within narrow backazimuthal ranges for a variety of cutoff frequencies. The eastern stack (A) includes data from backazimuths 75–107°; The western stack (B) includes data from backazimuths 255–285°. P_{Ms} is clear in all frequencies on both radial and transverse components, while P_{Hs} is primarily seen on the transverse component. At the lowest frequency RFs, P_{Hs} arrives from the west 0.3 s earlier than from the east (see also Fig. 5). Time-alignment of P_{Hs} is better at high frequencies.

2.0 Hz (Fig. 4). Also, the transverse component has more azimuthal continuity than the radial, which is poorly resolved between backazimuths 90° and 200°. Both the timing and pulse shape of the P_{Hs} phase vary with backazimuth; arrivals from the west are earlier and more complex (Fig. 5). Note that differences in P_{Hs} timing are more prominent at longer periods (Fig. 4). The transverse component of the P_{Hs} undergoes a

polarity reversal between backazimuths 150 and 220°, and again between backazimuths 320 and 30°, very similar to the behavior of P_{Ms} .

Reverberations from interfaces at midcrustal depths may arrive within this 4–10 s time window, but are unlikely to contain two-lobed transversely polarized energy that is as strong as that observed here (Levin and Park, 1998). Also, where the phase is seen well [Fig. 2(B)] it displays modest

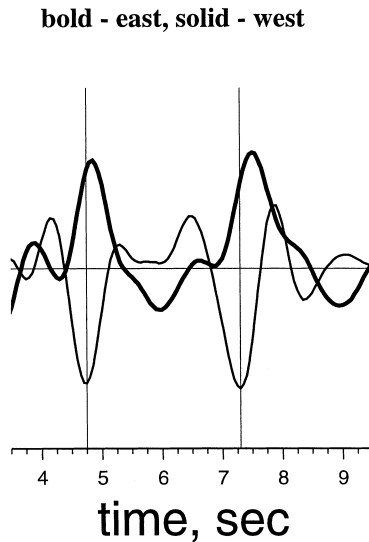


Fig. 5. Difference in timing of the transverse component of P_{HS} observed from opposite (east and west) directions. The RFs are lowpassed at 1 Hz.

negative moveout with increasing epicentral distance, as would be expected from an upgoing converted phase. On the basis of its backazimuthal provenance and epicentral distance moveout we interpret this phase as an upgoing Ps conversion from an impedance contrast ~ 70 km deep. Following Bostock (1997), we associate the P_{HS} phase with the Hales discontinuity.

Complexity in the pulse shape of the P_{HS} at higher frequencies (Fig. 4) suggests that Hales ‘discontinuity’ is in fact an anomalous region, either centered at 70 km depth or simply having its most prominent feature there. In addition to the phases discussed so far, a transversely polarized phase of opposite polarity appears between the P_{MS} and P_{HS} phases when low-pass values of 1 Hz and below are used. This phase disappears in the 2.0 Hz RF. In the following section we explore a range of possible models that would replicate this behavior.

3.2. Modeling

To model our observations we employ reflectivity calculations in one-dimensional horizontally-stratified anisotropic structures (Levin and Park,

1997a,b). Although some dip of the seismic interfaces is possible, the radial portions of P_{MS} and P_{HS} are too small for the transverse-polarized signals to be caused strictly, or even largely, by out-of-plane refraction from a dipping interface. Instead, we interpret the transverse RFs to be caused by anisotropy, which we model as having hexagonal symmetry. Waveforms obtained by stacking all RFs within a narrow backazimuthal bin are treated as ‘data’ to be fit through trial-and-error forward modeling. We utilize systematic backazimuthal variations within the RAYN RFs to guide our choice of forward modeling parameters.

We computed reflectivity seismograms for upgoing compressional pulses arriving from backazimuths 90° and 270° with phase velocity of 20 km s^{-1} ($\sim 24^\circ$ incidence angle within the subcrustal lithosphere). We estimated RFs from these synthetics to compare with data-derived RFs. Using results from active source work studies (Mooney et al., 1985) as a guide, we constructed an isotropic velocity model for RAYN that captures the major features of the long-period RFs (Fig. 6). Radial RFs may be fit with a three-layer crustal model containing a thin low-velocity layer on top, a mid-crustal interface at 21 km, and the Moho at 41 km (Table 1). Other velocity models for Arabia derived from the RF technique (Sandvol et al., 1998; Al-Amri, 1999) and surface-wave dispersion analysis (Rodgers et al., 1999) tend to confirm that the lower 20–25 km of the crust has relatively high seismic velocity.

The low-velocity surface layer must be thicker on the western side to yield the prominent negative pulse seen on radial RFs there. At first glance this behavior is counterintuitive, since the sediments of the Arabian Platform lie to the east of RAYN. However, the low-velocity layer most likely corresponds to a combination of sediment cover plus a weathered interval of the basement rocks. The positive pulse in synthetic-derived RFs at 9 s is a multiple reverberation from the midcrustal (21 km) interface in our model. Its absence in data suggests that the upper crust under Ar-Rayn has structural complexity that defocusses this multiple pulse.

Observed RFs vary greatly with backazimuth in the time window between 2 and 3 s [Fig. 3(A)],

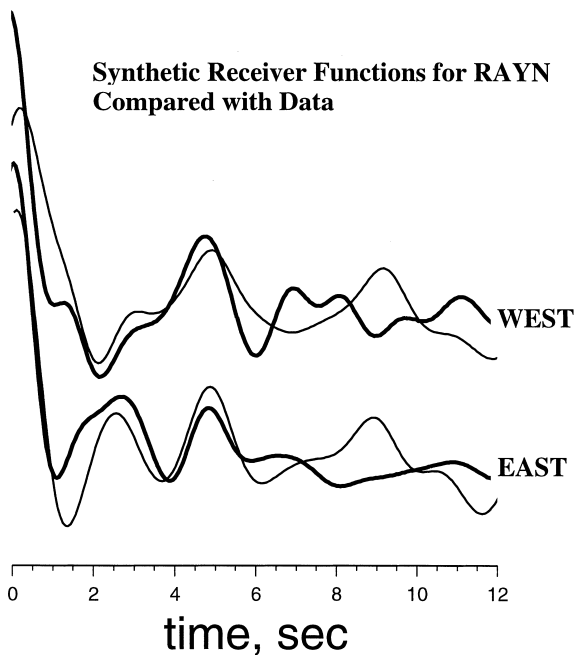


Fig. 6. Synthetic radial RFs (thin lines) computed in simple isotropic models (Table 1) that reproduce general features of the eastern and western RF stacks (bold lines). All waveforms are lowpassed at 0.5 Hz. The near-surface low-velocity layer must be thicker on the western side to yield the prominent negative pulse seen in the western RF stack. The positive pulse in synthetic-derived RFs at 9 s is a multiple reverberation from the midcrustal (21 km) interface in our model. Its absence in the data suggests that structural complexity of the crust above it defocusses the multiple pulse.

Table 1
Vertical profile of seismic properties consistent with radial RFs at RAYN^a

Depth (km)	V_p (km s ⁻¹)	V_s (km s ⁻¹)	ρ (g cm ⁻³)
1.2/2.8	5.0	2.85	2.2
21	6.3	3.7	2.7
41	7.0	4.0	2.9
72	8.15	4.7	3.1
∞	8.3	4.8	3.3

^a Isotropic velocity and density values for RAYN model. Values in the first column define lower boundaries of model layers. Top layer is thicker for western observations

where one would expect arrivals from mid-crustal interfaces, and much transversely polarized energy is seen. However, the azimuthal dependence of the

transverse RFs within this time window are less clear than in the case of P_{MS} and P_{HS} , especially at higher frequencies. Badri (1991) identified strong mid-crustal features, potentially with significant dip, along the refraction line crossing the Ar Rayn terrane. Since strongly dipping interfaces and lateral heterogeneity can also generate transversely-polarized Ps conversions, we chose not to model Ps scattered energy prior to P_{MS} in terms of flat-layered anisotropic features.

As discussed above, patterns of azimuthal variation in the transverse components of P_{MS} and P_{HS} are likely a consequence of anisotropy. These patterns may be simulated with reasonable fidelity by introducing anisotropy on the order of 5% at velocity contrasts located at 41 and 72 km. Fig. 7 displays a transmissivity response predicted for the model (discussed in detail below) with two anisotropic zones. To reproduce the two-lobed nature of the observed pattern under the assumption of hexagonally-symmetric anisotropy we use symmetry axes that are tilted 50° from the vertical. We chose to use anisotropy with a fast axis, as would be appropriate for LPO in olivine-rich mantle peridotite (Zhang and Karato, 1995). In the example shown we restricted the symmetry axes of anisotropy to share the same N–S strike. Qualitatively similar fits to data may be obtained if the symmetry-axis azimuth of either mantle layer deviates by 10°.

A difference in P_{HS} timing between eastern and western stacks (Fig. 5) may be accommodated by decreasing the depth of the velocity contrast from 72 to 68 km while keeping velocity values fixed. Given the tradeoff of velocity and depth in RF modeling a similar effect could be achieved by altering the ratio of P and S wave velocities as well. However, note that the sharpest features of P_{HS} in the highest frequency RF stacks align well in time. The frequency dependence of the time mismatch (Fig. 4) suggests that the Hales discontinuity itself may lie at a fixed depth, but that the surrounding vertical gradients in velocity and anisotropy have some azimuthal variation.

In observed transverse RFs both P_{MS} and P_{HS} have distinctively one-sided pulse shapes that are either positive or negative depending on backazimuth. P-SH converted waves with such pulse shapes are expected when mode conversion takes

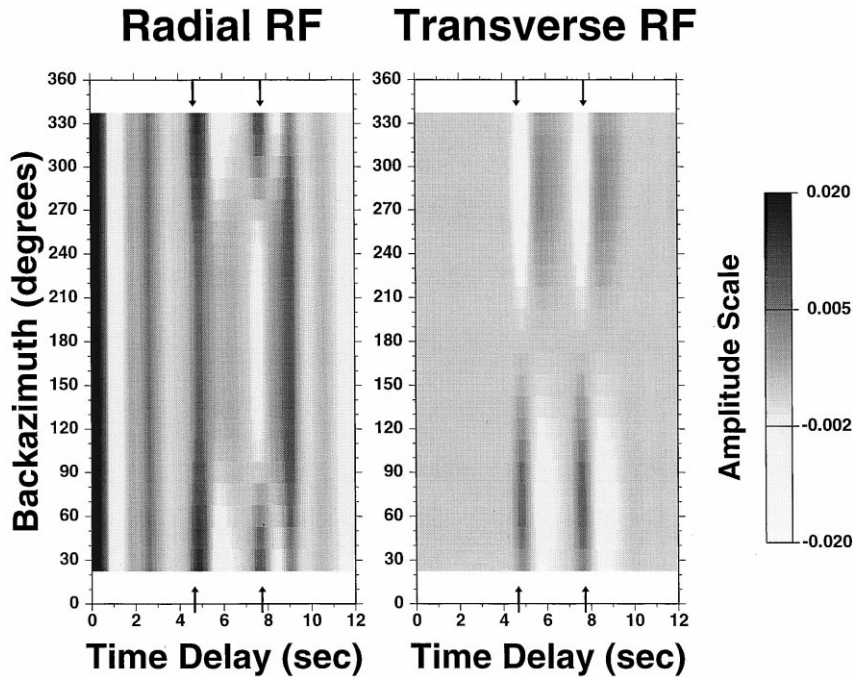


Fig. 7. Transmissivity response image for a model containing anisotropic zones that extend downward from the Moho and Hales discontinuities (cf. Fig. 8). Computations were performed for a compressional pulse arriving from a set of regularly-spaced backazimuths with a phase velocity of 20 km s^{-1} . Spectrum of synthetic-seismogram RFs is limited at 1 Hz. Phases P_{MS} and P_{HS} are identified by arrows.

place at an isolated first-order velocity discontinuity. Since conversions from the top and bottom of a thick anisotropic layer would have opposite polarities (Levin and Park, 1998), we model P_{MS} and P_{HS} as arising from independent anisotropic features. Figs. 8 and 9 illustrate a range of models. We show computations only for the eastern backazimuth, for comparison with Fig. 4(A). Reversing the backazimuth of an incident waveform would lead to reverse polarity on the transverse component. Clearly, the long-period behavior of the RAYN RFs is captured fairly well by all models. However, expanding the spectrum of synthetics to 2 Hz, we can see significant differences in the predicted waveforms.

Model A contains two layers of anisotropy, with opposite directions of axis tilt from the vertical (50° toward the south in the upper layer, 50° toward the north in the lower layer). Models B and C employ linear gradients in anisotropic intensity, and Model D has a quadratic dependence of

anisotropy strength on depth. Gradational changes in anisotropy are implemented as sequences of 20 thin layers for each gradient. Orientation of the anisotropic axis stays fixed throughout the sequence. In Model B the axis tilt is identical to Model A (south on top, north on the bottom). In Model C both anisotropic zones have the symmetry-axis tilting from the vertical 50° toward the south. In Model D the anisotropy-axis in the top zone tilts to the north while the axis in the bottom sequence tilts to the south. It should be noted that the direction of symmetry-axis tilt depends on the choice of anisotropy type. Levin and Park (1998) show that mirror-image patterns of P-SH conversions are obtained when the sense of anisotropy (fast or slow along the axis) is reversed. For Model D the top layer of anisotropy falls within the crust, where anisotropy with a slow symmetry-axis is likely (e.g. due to fine-layering — see Levin and Park, 1997a). For slow-axis symmetry in the crust, a tilt to the south would match the observations.

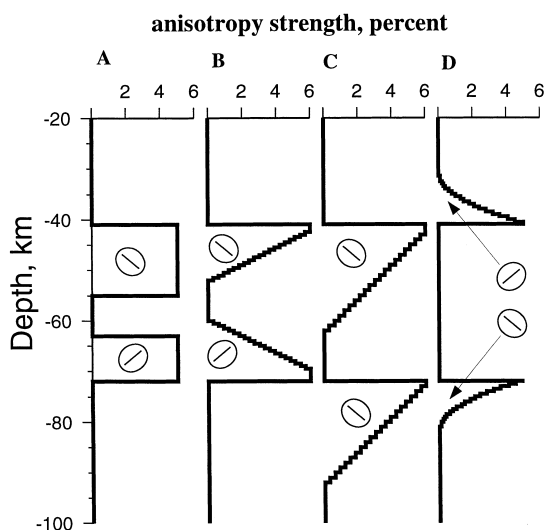


Fig. 8. Vertical profiles of anisotropy strength in the models we tested against RAYN RFs. Velocity and density values are shown in Table 1. Coffee-bean symbols show the orientation of symmetry-axis of anisotropy, and the resulting distribution of velocity, within each zone. Symmetry-axis tilt (from the vertical) toward the south is indicated by a symbol that tips to the left.

On the basis of qualitative comparison of Figs. 4(A) and 9 we believe that Model C yields synthetics that behave most like the observed RFs. The secondary pulses that develop at high frequency in models A and B are too large. Model D leads to pulses of the wrong polarity before P_{MS} and after P_{HS} , which are also larger than those seen in the data. The azimuthal pattern for RFs computed from Model C is shown in Fig. 7. The transverse component pattern is very similar to that on Fig. 3(A). Since the model was developed to match observations from the east, the radial component does not replicate a strong negative pulse seen in the western part of the observed pattern. It does show a broad positive arrival at the P_{HS} time, which is similar in behavior to the intermittent phase in Fig. 3(A).

What aspects of the forward modeling should be believed? A tilted axis of symmetry, striking roughly N–S, is required to match the two-lobed polarity of P_{MS} and P_{HS} in the context of hexagonally-symmetric anisotropy. We did not explore anisotropic models with orthorhombic, or more

complex, symmetry. We feel that our knowledge of how mineral fabric develops in deformed peridotite does not yet justify such additional complexity. The one-sided nature of P_{MS} and P_{HS} favor anisotropic zones that are bounded by a one sharp mantle-fabric gradient and one gradual mantle-fabric gradient. The values of parameters in our preferred Model C are not constrained tightly by our forward modeling exercise using RFs from eastern backazimuths, particularly the precise thickness and functional dependence of anisotropy gradients within the inferred shear zones. For instance, in Model D the anisotropic gradient beneath the Hales discontinuity is steeper than Model C, and this alteration changes the P_{HS} pulse to resemble better the RAYN RFs from western backazimuths.

4. Discussion

The transverse RFs at station RAYN imply sharp gradients in depth-dependent anisotropy in the shallow mantle, at the Moho and at the Hales discontinuity. The Hales ‘discontinuity’ beneath RAYN may actually be a $\lesssim 20$ km anisotropic zone, a conclusion also reached by Bostock (1998) for the Slave Province of Canada. Previous converted-phase studies, which typically involve longer period body waves, may have had insufficient resolution in depth to distinguish a finite zone of enhanced mantle fabric from a sharp discontinuity in material properties. Asymmetry in the RF pulses at 1–2 Hz suggest that the upper boundary of each shear zone is sharp, and the lower boundary gradational. A similar depth dependence in anisotropic strength was inferred by Bostock (1998) for the Slave Province, so the Hales ‘discontinuity’ nomenclature may be still be appropriate, as long as it refers to the top of the zone. The inferred symmetry axes of the anisotropy strike N–S, in general agreement with the fast shear wave direction inferred by Wolfe et al. (1999) for the Arabian shield on the basis of SKS splitting.

To check this relation between our RF analysis and the deeper structure we compiled records of SKS waves from RAYN with high S/N ratio, well distributed in backazimuth and with considerable

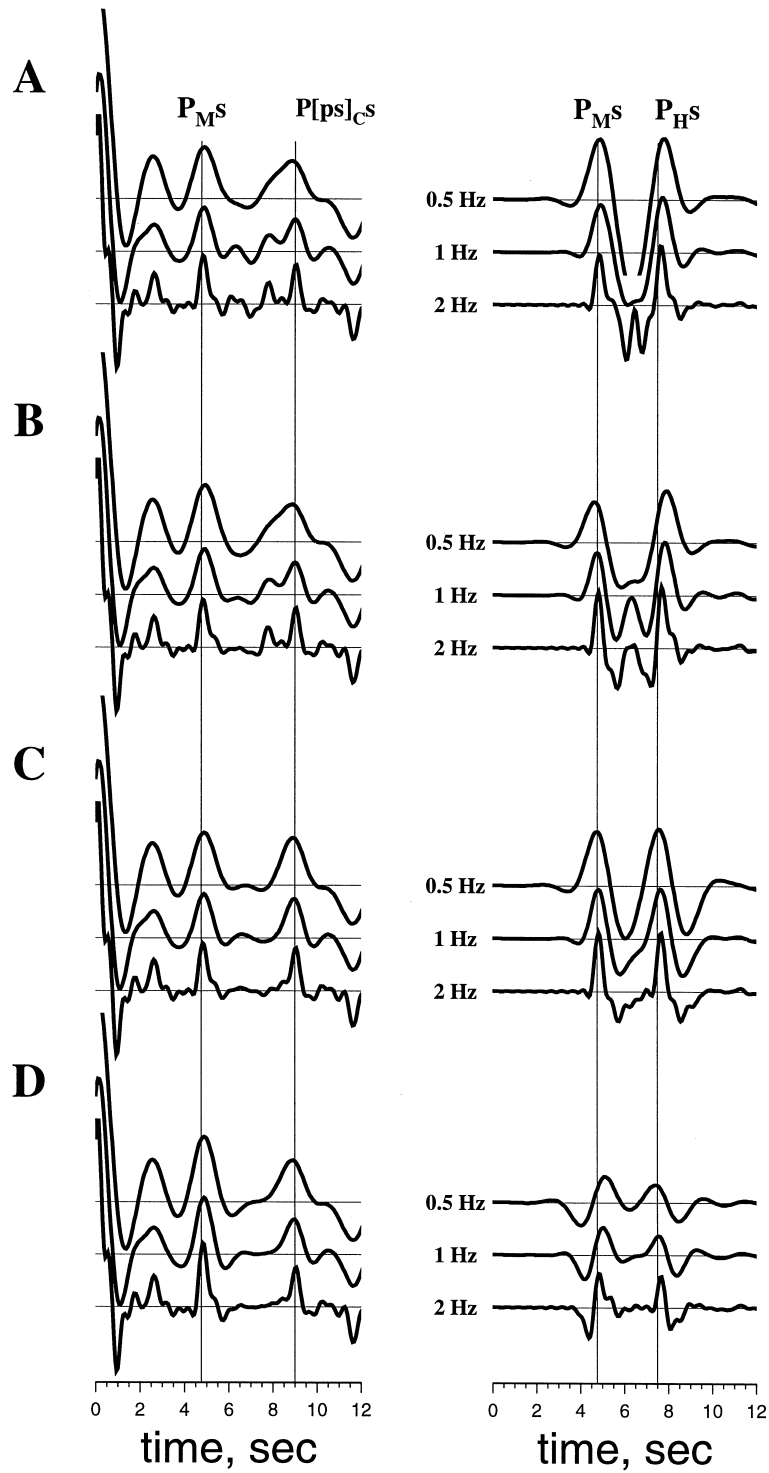


Table 2
Results of shear wave splitting analysis^a

Event (yyyy.jdy.hr)	Latitude (°)	Longitude (°)	Depth (km)	BAZ (°)	Distance (°)	Fast direction (°)	Delay (s)
1997.141.14	−20.44	169.29	57.0	98.2	128.1	48.3	0.74
1997.142.08	18.68	−101.60	70.0	319.9	126.9	4.9	0.64
1997.168.21	51.35	−179.33	33.0	26.3	95.4	153.4	0.66
1997.187.10	−30.06	−71.87	19.0	248.7	124.4	19.5	1.19
1997.245.12	3.85	−75.75	199.0	287.5	116.6	–	–
1997.332.23	−13.74	−68.79	586.0	266.2	117.5	23.4	0.77
1997.351.05	51.19	178.87	20.0	27.2	94.8	128.1	0.70
1997.356.02	−5.49	147.87	179.0	90.2	103.5	53.9	0.39
1998.010.08	14.37	−91.47	33.0	307.7	123.4	176.1	0.32
1998.030.12	−23.91	−70.21	42.0	255.5	121.7	30.4	1.09

^a Earthquake locations determined by National Earthquake Information center of the US Geologic Survey. Fast direction values are clockwise from north.

energy in the passband comparable to that of RFs (~ 1 Hz). The latter consideration is significant, as frequency dependence of SKS splitting observations have been both observed and predicted theoretically (Marson-Pidgeon and Savage, 1997; Savage, 1999). We found 10 suitable SKS phases in RAYN records from 1997 and 1998. Results of shear-wave splitting analysis utilizing a crosscorrelation technique (Levin et al., 1999) are presented in the inset of Fig. 1, and in Table 2. SKS phases arriving from the west and northwest yield fast directions close to N–S (note also a ‘null’ measurement at backazimuth 287°), while phases arriving from the northeast and east clearly do not.

Assuming that the anisotropy that splits SKS phases resides in the upper mantle [i.e., below Moho and above 400 km, see Silver (1996)], the regions affecting SKS phases (incidence angle in the upper mantle $\sim 10^\circ$) arriving from opposite directions (E and W) are separated by 50–150 km. Lateral variability in lithospheric strain beneath the Hales discontinuity is a likely explanation, perhaps related to the terranes composing the region, especially in view of the NNW strike of

regional tectonic boundaries (Fig. 1). The nearly N–S orientation seen from the west samples the region beneath the Najd faulting system. SKS phases from the east probe the upper mantle under the Ar Rayn block, which is of distinct tectonic origin, and may have been less affected by the Najd faulting. However, it should be noted that some form of multilayered anisotropy could also lead to our observations, and can not be excluded on the basis of this sparse dataset.

The variability in SKS observations suggests that the shear-wave splitting signal does not arise solely from the asthenospheric drag at the base of the continental plate, one of the hypotheses entertained by Wolfe et al. (1999). At the opposite extreme, if all mantle shear were restricted to lie above the Hales discontinuity, in a layer ~ 30 km thick, the anisotropy required to generate ~ 1 s birefringence in SKS phases would exceed 10%. In our preferred model for the RFs, anisotropy is restricted to $\lesssim 20$ km thin shear zones and is $\leq 6\%$. Synthetic SV pulses propagated upwards through our preferred velocity model exhibit no more than 0.1 s of splitting. We conclude that additional

Fig. 9. Synthetic seismograms for various anisotropy-depth profiles within the mantle lid (indicated by letters, cf. Fig. 8). Computations were performed for a P wave incident from the east, for comparison with Fig. 4(A). Velocity profile used in all computations is presented in Table 1. The 2 Hz RFs for Model C provide the best match to the one-sided pulses on the RAYN RFs from eastern backazimuths. A modest alteration in the anisotropic gradient beneath the Hales discontinuity in Model C, to resemble the Model D_e gradient, changes the P_HS pulse to resemble better the RAYN RFs from western backazimuths.

mantle fabric with N–S orientation resides in the lithosphere beneath the Hales.

The relation between the tectonic history of Arabia and our velocity/anisotropy profile for the RAYN RFs is not uniquely constrained. A correspondence between the Hales and a buried eclogitized oceanic crust (Bostock, 1998) cannot be ruled out completely, but two facts discourage this interpretation:

1. the N–S trend of the anisotropic symmetry-axis at the Hales is perpendicular to the presumed E–W vergence of terrane accretion in the late Proterozoic; and
2. both Moho and Hales have indistinguishable anisotropic trends, suggesting a contemporaneous deformation event.

We note, however, that the three-dimensional kinematics of oblique subduction and terrane accretion, the presumed mechanism for the assembly of the Arabian shield, are not known in detail. It is possible that an eclogitized oceanic crust, possibly under the influence of subducted volatiles, could act as a detachment zone for the trench-parallel motion of an accreted block.

We propose an alternate scenario in which shear concentrations at the Hales and Moho boundaries were guided by a depth-dependent rheology within the lithosphere (Fig. 10). Metamorphism of its bounding ophiolites suggests that the Ar Rayn terrane accreted to the Arabian Shield at 680 Ma (Al-Saleh et al., 1998) along the Al-Amar suture zone striking approximately N340°W. Subsequent

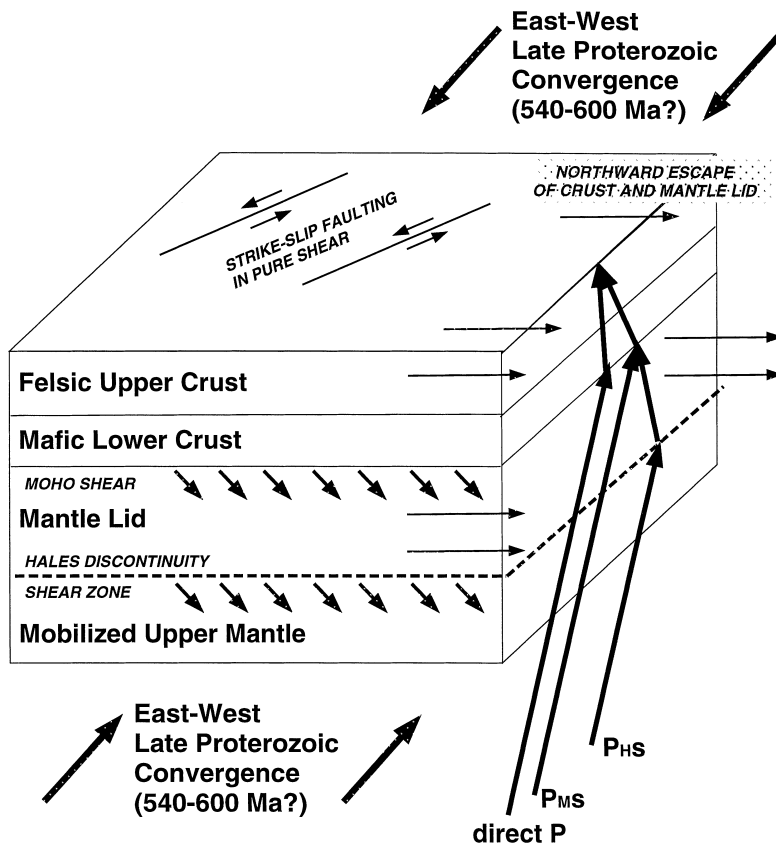


Fig. 10. Schematic diagram illustrating the development of shear zones within the upper mantle beneath the Ar Rayn terrane of the Arabian Shield, during an episode of northward 'tectonic escape' in the late Proterozoic. Arrows beneath the Moho and Hales discontinuities indicate the location and direction of lattice-preferred orientation in olivine grains suggested by Model C.

metamorphism indicates that, near 600 Ma, the region was affected by another continent–continent collision further to the east. During the following intracratonic stage, the Najd fault system developed to the south of Ar-Rayn terrane, striking roughly N300°W, and accumulated as much as 400 km of left-lateral slip (Davies, 1984). The different strike of the post-orogenic faulting suggests an evolution in mantle deformation. Terranes that accrete to continents via oblique subduction tend to slide parallel to the accretion boundary along transcurrent faults, suggesting simple shear in the underlying mantle. After suture and amalgamation of terranes, the new continental lithosphere may deform in pure shear in response to the indentation by a rigid body, for example, as envisaged for the present-day collision of India with Asia. Under this ‘escape tectonics’ scenario (Stern, 1994), the motion of the Ar Rayn block, ‘riding’ along the northern face of the Najd shear zone, would have been in a direction close to present-day N–S, while the shear zone itself displaced along a NW strike. A similar geometric relation has been noted at the western boundary of the Tibetan Plateau, where bounding transcurrent faults mediate the eastward motion of the Plateau (Holt and Haines, 1993), and in central Anatolia, which is moving west toward the Aegean Sea in response to the collision of Arabia with Eurasia (Jackson and McKenzie, 1984). Holt (2000) has noted that the strong E–W anisotropic fast axis in Tibet, as inferred from SKS splitting (McNamara et al., 1994; Hirn et al., 1998), aligns with the escape direction of the surface block.

We hypothesize that a relatively strong mantle ‘lid’ between the Moho and the Hales discontinuities migrated northward as the escape-tectonics ‘block’ during the last stages of terrane accretion for the Arabian Shield. The lid would have been bounded at top and bottom, respectively, by lower crust and peridotite layers with thermally activated lower viscosity. The lower crust detachment zone allowed larger blocks of Arabian upper crust to deform along NW–SE trending surface fault systems. Mafic underplating, however, may have erased or obscured any anisotropy associated with this deformation, aside from the strained layer that we infer just below the Moho. The detachment

zone at the Hales could arise as the scar left by a departed orogenic root (Molnar et al., 1993) or a delamination surface (Schott and Schmeling, 1998). However, trace-element studies of Arabian shield volcanism argue against the contribution of asthenosphere 600 Ma or younger to post-orogenic igneous activity (Ibrahim and McCourt, 1995; Stein and Goldstein, 1996). The Arabian lithosphere beneath the Hales may have been remobilized in the aftermath of the continent–continent collision, and suffered only a partial removal of the orogenic root. Turner et al. (1996) appeal to a similar ‘lithospheric thinning’ scenario to explain the enriched trace-element signature of Cenozoic post-uplift volcanism in Tibet.

Layered rheological models were proposed by Chen and Molnar (1983) to explain the lower crustal seismicity gap of many continental collision zones, and by Jin et al. (1994) to explain the existence of two distinct wavelengths of correlated ridge–trough gravity and topography variations in the Tibet region. The stiff mantle lid in Jin et al. (1994), responsible for 500 km wavelength spatial variations in Tibet, is inferred to have thickness ~40 km, comparable to the thickness of the Arabian mantle above the Hales discontinuity. This seismic feature, observed in many continental regions, may in many instances be a relict of a thermally-controlled mantle detachment characteristic of continental accretion processes. A related scenario is invoked by Jones and Phinney (1998) to explain Ps converted energy at 7–9 s delay in small-array RFs from the Sierra Nevada mountains. In their scenario, asthenospheric upwelling beneath the mountain range, creeping outward from the delaminated Basin-and-Range province in the western United States, is largely responsible for the Sierras’ current topography. Proterozoic stretch marks from similar dynamics may be preserved within the shallow lithosphere of the Arabian Shield. The RF study of Sandvol et al. (1998) suggests a variable depth to an interface in the Hales depth range across the southeastern portion of the Shield, but does not analyze the transverse component. Our experience with RAYN, for which Sandvol et al. (1998) reported no P_{HS} phase, suggests that the azimuthal dependence of the transverse RF is a crucial constraint

on the relict strains embedded within continental lithosphere.

5. Conclusions

On the basis of teleseismic RF analysis we identify two $\lesssim 20$ km thick zones within the subcrustal lithosphere on the eastern edge of the Arabian Shield where seismic anisotropy appears to be present. Anisotropy is associated with the crust-mantle transition, and with another anomalous region ~ 70 km deep, which we interpret as containing the Hales discontinuity. Azimuthal patterns and frequency dependence of pulse shapes of observed P–SH converted waves suggest that both zones are bounded by discontinuities in anisotropic properties on one side, and by smooth gradients on another. In our preferred model anisotropic zones extend downward from the Moho and the Hales discontinuities. Within both zones the anisotropic symmetry axes, indicative of systematic fabric in the olivine-dominated upper mantle material, are oriented along the N–S direction ($\pm 10^\circ$), and are tilted 50° to the south.

We interpret our findings as evidence for thin shear zones within the mantle lithosphere, developed after the assembly of the Arabian Shield during a late Proterozoic continent–continent collision. Post-collisional tectonics created the Najd fault system and involved the Ar-Rayn block in an ‘escape tectonics’ episode along the trajectory that would be close to present-day N–S direction. Preservation of these shear zones for ~ 500 My within the upper mantle is in good agreement with geochemical evidence for common tectonic history of the crust and upper mantle composing the Arabian Shield.

Although recognised globally, the details of the Hales discontinuity appear to be tied to the tectonic history of a specific location (Arabian shield, Slave craton). Therefore, a single origin of this seismic feature, analogous to the mineral phase changes at 420 and 670 km depth, may be hard to constrain. Rather, we hypothesize that the typical depth range of the Hales discontinuity (60–90 km) is where tectonic events often leave their ‘marks’ in the continental lithosphere, perhaps indicating the minimum thickness of the stiff mantle lid in orogenic events.

Acknowledgements

This work has been supported by Defense Threat Reduction Agency Contract DSWA01-98-011 and NSF Grant No. EAR-9805206. Mark Brandon alerted us to Turner et al. (1996). Arthur Rodgers and an anonymous reviewer provided helpful comments. We used GMT software (Wessel and Smith, 1991) to prepare the figures.

References

- Abbott, D., 1992. The case for accretion of the tectosphere by buoyant subduction. *Geophys. Res. Lett.* 18, 585–588.
- Abdel-Rahman, A.-F.M., 1995. Tectonic-magmatic stages of shield evolution, the Pan-African Belt in northeastern Egypt. *Tectonophysics* 242, 223–240.
- Abdelsalam, M.G., Stern, R.J., 1996. Sutures and shear zones in the Arabian–Nubian Shield. *J. Afr. Earth Sci.* 23, 289–310.
- Abers, G.A., 1998. Array measurements of phases used in receiver-function calculations: importance of scattering. *Bull. Seism. Soc. Am.* 87, 313–318.
- Al-Amri, A., 1999. The crustal and upper-mantle structure of the interior Arabian Platform. *Geophys. J. Int.* 136, 421–430.
- Al-Saleh, A.M., Boyle, A.P., Mussett, A.E., 1998. Metamorphism and $^{40}\text{Ar}/^{39}\text{Ar}$ dating of the Halaban Ophiolite and associated units, evidence for two-stage orogenesis in the eastern Arabian Shield. *J. Geol. Soc. London* 155, 165–175.
- Ammon, C.J., 1991. The isolation of receiver effects from teleseismic *P* waveforms. *Bull. Seism. Soc. Am.* 81, 2504–2510.
- Badri, M., 1991. Crustal structure of central Saudi Arabia from seismic refraction profiling. *Tectonophysics* 185, 357–374.
- Bellefleur, G., Calvert, A.J., Chouteau, M.C., 1997. A link between deformation history and the orientation of reflective structures in the 2.68–2.83 Ga Opatca belt of the Canadian Superior Province. *J. Geophys. Res.* 102, 15243–15257.
- Bentor, Y.K., 1985. The crustal evolution of the Arabo-Nubian massif with special reference to the Sinai peninsula. *Precambrian Res.* 28, 1–74.
- Benz, H.M., McCarthy, J., 1994. Evidence for an upper mantle low velocity zone beneath the southern Basin and Range–Colorado Plateau transition zone. *Geophys. Res. Lett.* 21, 509–512.
- Berhe, S.M., 1997. The Arabian–Nubian shield. In: De Wit, M.J., Ashwal, L.D. (Eds.), *Greenstone Belts*. Oxford University Press, Oxford, pp. 761–771.
- Bird, P., 1979. Continental delamination and the Colorado Plateau. *J. Geophys. Res.* 84, 7561–7571.
- Bonavia, F.F., Chorowicz, J., Collet, B., 1995. Have wet and dry Precambrian crust largely governed Cenozoic intraplate

- magmatism from Arabia to East Africa? *Geophys. Res. Lett.* 22, 2337–2340.
- Bostock, M.G., 1997. Anisotropic upper-mantle stratigraphy and architecture of the Slave craton. *Nature* 390, 393–395.
- Bostock, M.G., 1998. Mantle stratigraphy and the evolution of the Slave province. *J. Geophys. Res.* 103, 21183–21200.
- Camp, V.E., Roobol, M.J., 1992. Upwelling asthenosphere beneath western Arabia and its regional implications. *J. Geophys. Res.* 97, 15255–15271.
- Chen, W.-P., Molnar, P., 1983. Focal depths of intracontinental and intraplate earthquakes and their implications for the thermal and mechanical properties of the lithosphere. *J. Geophys. Res.* 88, 4183–4214.
- Davies, F.B., 1984. Strain analysis of wrench faults and collision tectonics of the Arabian–Nubian shield. *J. Geol.* 82, 37–53.
- Earle, P., Shearer, P., Zandt, G., Walter, W., 1994. A global survey for the 80-km discontinuity utilizing three-component broadband data (abstract). *EOS Trans. AGU* 75, 435.
- Fuchs, K., 1983. Recently formed elastic anisotropy and petrological models for the continental subcrustal lithosphere in southern Germany. *Phys. Earth Planet. Int.* 31, 93–118.
- Fuchs, K., Vinnik, L.P., 1982. Investigation of the subcrustal lithosphere and asthenosphere by controlled source seismic experiments of long-range profiles. In: Palmason, G. (Ed.), *Continental and Oceanic Rifts*. Geodynamics Series vol. 8. American Geophysical Union, Washington DC, pp. 81–98.
- Gurrola, H., Baker, F.G., Minster, J.B., 1995. Simultaneous time-domain deconvolution with application to the computation of receiver functions. *Geophys. J. Int.* 120, 537–543.
- Hales, A.L., 1969. A seismic discontinuity in the lithosphere. *Earth Planet. Sci. Lett.* 7, 44–46.
- Hales, A.L., Muirhead, K.J., Rynn, J.M., Gettrust, J.F., 1975. Upper-mantle travel times in Australia — a preliminary report. *Phys. Earth Planet. Int.* 11, 109–118.
- Hirn, A., Diaz, J., Sapin, M., Veinante, J.-L., 1998. Variation of shear-wave residuals and splitting parameters from array observations in southern Tibet. *Pure Appl. Geophys.* 151, 407–431.
- Holt, W.E., 2000. Correlated crust and mantle strain fields in Tibet. *Geology* 28, 67–70.
- Holt, W.E., Haines, A.J., 1993. Velocity fields in deforming Asia from the inversion of earthquake-released strains. *Tectonics* 12, 1–20.
- Ibrahim, K.M., McCourt, W.J., 1995. Neoproterozoic granitic magmatism and tectonic evolution of the northern Arabian Shield, evidence from Southwest Jordan. *J. Afr. Earth Sci.* 20, 103–118.
- Jackson, J., McKenzie, D., 1984. Active tectonics of the Alpine–Himalayan belt between western Turkey and Pakistan. *Geophys. J. R. Astron. Soc.* 77, 185–264.
- Jin, Y., McNutt, M.K., Zhu, Y., 1994. Evidence from gravity and topography data for folding of Tibet. *Nature* 371, 669–674.
- Johnson, P.R., Stewart, I.C. F., 1995. Magnetically inferred basement structure in central Saudi Arabia. *Tectonophysics* 245, 37–52.
- Jones, C.H., Phinney, R.A., 1998. Seismic structure of the lithosphere from teleseismic converted arrivals observed at small arrays in the southern Sierra Nevada and vicinity, California. *J. Geophys. Res.* 103, 10065–10090.
- Kosarev, G.L., Makeyeva, L.I., Vinnik, L.P., 1984. Anisotropy of the mantle inferred from observations of *P* to *S* converted waves. *Geophys. J. R. Astron. Soc.* 76, 209–220.
- Langston, C.A., 1981. Evidence for the subducting lithosphere under southern Vancouver Island and western Oregon from teleseismic *P* wave conversions. *J. Geophys. Res.* 86, 3857–3866.
- Levin, V., Park, J., 1997a. Crustal anisotropy beneath the Ural mountains foredeep from teleseismic receiver functions. *Geophys. Res. Lett.* 24, 1283–1286.
- Levin, V., Park, J., 1997b. *P-SH* conversions in a flat-layered medium with anisotropy of arbitrary orientation. *Geophys. J. Int.* 131, 253–266.
- Levin, V., Park, J., 1998. A *P-SH* conversion in layered media with hexagonally symmetric anisotropy: a cookbook. *Pure Appl. Geophys.* 151, 669–697.
- Levin, V., Menke, W., Park, J., 1999. Shear wave splitting in Appalachians and Urals: a case for multilayered anisotropy. *J. Geophys. Res.* 104, 17975–17994.
- Levin, V., Park, J., Brandon, M.T., Menke, W., 2000. Thinning of the upper mantle during late Paleozoic Appalachian orogenesis. *Geology* 29, 239–242.
- Marson-Pidgeon, K., Savage, M.K., 1997. Frequency-dependent anisotropy in Wellington, New Zealand. *Geophys. Res. Lett.* 24, 3297–3300.
- McNamara, D.E., Owens, T.J., Silver, P.G., Wu, F.T., 1994. Shear wave anisotropy beneath the Tibetan Plateau. *J. Geophys. Res.* 99, 13655–13665.
- Meissner, R., Mooney, W., 1998. Weakness of the lower continental crust: a condition for delamination, uplift and escape. *Tectonophysics* 296, 47–60.
- Molnar, P., England, P., Martinod, J., 1993. Mantle dynamics, uplift of the Tibetan Plateau, and the Indian monsoon. *Rev. Geophys.* 31, 357–396.
- Mooney, W.D., Gettings, M.E., Blank, H.R., Healy, J., 1985. Saudi Arabian deep refraction profile, a traveltimes interpretation for crustal and upper mantle structure. *Tectonophysics* 111, 173–246.
- Park, J., Levin, V., 2000. Receiver functions from multiple-taper spectral correlation estimates. *Bull. Seism. Soc. Am.* (submitted for publication).
- Pavlenkova, N.I., 1996. General features of the uppermost mantle stratification from long-range seismic profiles. *Tectonophysics* 264, 261–278.
- Prodehl, C., 1985. Interpretation of a seismic refraction survey across the Arabian Shield in western Saudi Arabia. *Tectonophysics* 111, 247–282.
- Revenaugh, J., Jordan, T.H., 1991. Mantle layering from ScS reverberations 3. The upper mantle. *J. Geophys. Res.* 96, 19781–19810.
- Rodgers, A.J., Walter, W.R., Mellors, R.J., Al-Amri, A.M.S., Zhang, Y.-S., 1999. Lithospheric structure of the Arabian Shield and Platform from complete regional waveform mod-

- elling and surface wave group velocities. *Geophys. J. Int.* 138, 871–878.
- Sacks, I.S., 1983. The subduction of young lithosphere. *J. Geophys. Res.* 88, 3355–3366.
- Sandvol, E., Seber, D., Barazangi, M., Vernon, F.L., Mellors, R., Al-Amri, A., 1998. Lithospheric seismic velocity discontinuities beneath the Arabian Shield. *Geophys. Res. Lett.* 25, 2873–2876.
- Savage, M.K., 1998. Lower crustal anisotropy or dipping boundaries? Effects on receiver functions and a case study in New Zealand. *J. Geophys. Res.* 103, 15069–15087.
- Savage, M.K., 1999. Seismic anisotropy and mantle deformation, what have we learned from shear wave splitting? *Rev. Geophys.* 37, 65–106.
- Schott, B., Schmeling, H., 1998. Delamination and detachment of a lithospheric root. *Tectonophysics* 296, 225–247.
- Silver, P.G., 1996. Seismic anisotropy beneath the continents: probing the depths of geology. *Ann. Rev. Earth Planet. Sci.* 24, 385–432.
- Stein, M., Goldstein, S.L., 1996. From plume head to continental lithosphere in the Arabian–Nubian Shield. *Nature* 382, 773–778.
- Stein, M., Navon, O., Kessel, R., 1997. Chromatographic metasomatism of the Arabian–Nubian lithosphere. *Earth Planet. Sci. Lett.* 152, 75–91.
- Stern, R.J., 1994. Arc-assembly and continental collision in the Neoproterozoic East African Orogen, implications for the consolidation of Gondwanaland. *Ann. Rev. Earth Planet. Sci.* 22, 319–351.
- Stoeser, D.B., Camp, V.E., 1985. Pan-African microplate accretion of the Arabian Shield. *Geol. Soc. Am. Bull.* 96, 817–826.
- Thybo, H., Perchuc, E., 1997. The seismic 8° discontinuity and partial melting in continental mantle. *Science* 275, 1626–1629.
- Turner, S., Arnaud, N., Liu, J., Rogers, N., Hawkesworth, C., Harris, N., Kelley, S., Van Calsteren, P., Deng, W., 1996. Post-collision, shoshonitic volcanism on the Tibetan plateau: implications for convective thinning of the lithosphere and the source of ocean island basalts. *J. Petrol.* 37, 45–71.
- Wessel, P., Smith, W.H. F., 1991. Free software helps map and display data. *EOS, Trans. AGU* 72, 441.
- Whitehouse, M.J., Windley, B.F., Ba-Bttat, M.A.O., Fanning, M.C., Rex, D.C., 1998. Crustal evolution and terrane correlation in the eastern Arabian Shield, Yemen, geochronological constraints. *J. Geol. Soc. London* 155, 281–295.
- Willett, S.D., Beaumont, C., 1994. Subduction of Asian lithospheric mantle beneath Tibet inferred from models of continental collision. *Nature* 369, 642–645.
- Windley, B.F., Whitehouse, M.J., Ba-Bttat, M.A.O., 1996. Early Precambrian gneiss terranes and Pan-African island arcs in Yemen, crustal accretion of the eastern Arabian Shield. *Geology* 24, 131–134.
- Wolfe, C.J., Vernon, F.L., Al-Amri, A., 1999. Shear-wave splitting across western Saudi Arabia: the pattern of upper-mantle anisotropy at a Proterozoic shield. *Geophys. Res. Lett.* 26, 779–782.
- Zandt, G., Randall, G.E., 1985. Observations of shear-coupled *P* waves. *Geophys. Res. Lett.* 12, 565–568.
- Zhang, S., Karato, S., 1995. Lattice preferred orientation of olivine aggregates deformed in simple shear. *Nature* 375, 774–777.
- Zhang, Y.S., Tanimoto, T., 1993. High-resolution global upper mantle structure and plate tectonics. *J. Geophys. Res.* 98, 9793–9823.
- Zhang, Z., Lay, T., 1993. Investigation of upper mantle discontinuities near northwestern Pacific subduction zones using precursors to *sSH*. *J. Geophys. Res.* 98, 4389–4405.